Journal of Chromatography A, 1436 (2016) 100–108

Contents lists available at ScienceDirect

Journal of Chromatography A

journal homepage: www.elsevier.com/locate/chroma

Improving permeability and chromatographic performance of poly(pentaerythritol diacrylate monostearate) monolithic column *via* photo-induced thiol-acrylate polymerization

Hongwei Wang[a,b,c], Junjie Ou[b,*], Jingyao Bai[b], Zhongshan Liu[b,c], Yating Yao[b,c], Lianfang Chen[b,c], Xiaojun Peng[a], Hanfa Zou[b,*]

[a] State Key Laboratory of Fine Chemicals, Dalian University of Technology, Dalian 116024, China
[b] Key Laboratory of Separation Science for Analytical Chemistry, National Chromatographic R&A Center, Dalian Institute of Chemical Physics, Chinese Academy of Sciences, Dalian 116023, China
[c] University of Chinese Academy of Sciences, Beijing 100049, China

ARTICLE INFO

Article history:
Received 2 December 2015
Received in revised form 18 January 2016
Accepted 23 January 2016
Available online 30 January 2016

Keywords:
Polymeric monoliths
Pentaerythritol diacrylate monostearate
Trimethylolpropane tris(3-mercaptopropionate)
Thiol-acrylate polymerization
2,2-Dimethoxy-2-phenylacetophenone
Photoinitiated

ABSTRACT

A simple approach was developed for rapid preparation of polymeric monolithic columns in UV-transparent fused-silica capillaries *via* photoinitiated thiol-acrylate polymerization of pentaerythritol diacrylate monostearate (PEDAS) and trimethylolpropane tris(3-mercaptopropionate) (TPTM) within 10 min, in which the acrylate homopolymerized and copolymerized with the thiol simultaneously. The morphology, permeability and chromatographic performance of the resulting poly(PEDAS-*co*-TPTM) monoliths were studied. It could be observed from SEM that the morphology of poly(PEDAS-*co*-TPTM) monolith was rather different from that of poly(PEDAS) monolith, which was fabricated *via* photo-induced free radical polymerization using PEDAS as the sole monomer. Compared with poly(PEDAS) monolith, poly(PEDAS-*co*-TPTM) monolith possessed better permeability when they were fabricated under the same preparation conditions. By adjusting the composition of porogenic solvents, poly(PEDAS-*co*-TPTM) monolith exhibited lower plate heights (15.7–17.7 μm) than poly(PEDAS) monolith (19.1–37.9 μm) in μLC. In addition, 66 unique peptides were positively identified on poly(PEDAS-*co*-TPTM) monolith when tryptic digest of four proteins was separated by μLC-MS/MS, demonstrating its potential in proteome analysis.

1. Introduction

Since monolithic columns emerged in the 1990s, they have received great attention in the separation field. Compared with packed columns, monoliths are easier and faster to fabricate in a capillary format, do not require retaining frits, exhibit faster mass transfer (depending on the monolith morphology), lower pressure drop, and richer chemistry for variety of selectivity [1–7]. Among three kinds of monoliths, namely, organic monoliths, silica-based inorganic monoliths and organic-silica hybrid monoliths, the porous polymeric monoliths (PPMs) are remarkably versatile as they can be readily prepared with different pore sizes, varying porosity, and a wide variety of chemical functionalities through the control of precursors and chemistry during polymerization, becoming important materials in separation science, sample enrichment and biocatalysis [8–15].

Particularly, PPMs are ideal media for the separation of large molecules, such as proteins, peptides, nucleic acids and synthetic polymers, due to their good convective mass transfer and broad selectivity. However, PPMs typically demonstrate low column efficiency for the separation of small molecules under LC conditions, which has been attributed to their high gel porosity and low mesopores (2–50 nm) volume. Gel porosity corresponds to micropores (<2 nm) within the solvated monolithic stationary phase, which does not affect the separation of large molecules, but plays vitally important roles on the separation of small molecules [16,17]. Great efforts have been made to improve the chromatographic performance of PPMs for the separation of small molecules, for example, optimizing the preparation conditions or adopting hyper-crosslinking technique [18–22].

* Corresponding authors. Fax: +86 411 84379620.
E-mail addresses: junjieou@dicp.ac.cn, oujunjie2002@163.com (J. Ou), hanfazou@dicp.ac.cn (H. Zou).

http://dx.doi.org/10.1016/j.chroma.2016.01.063
0021-9673/

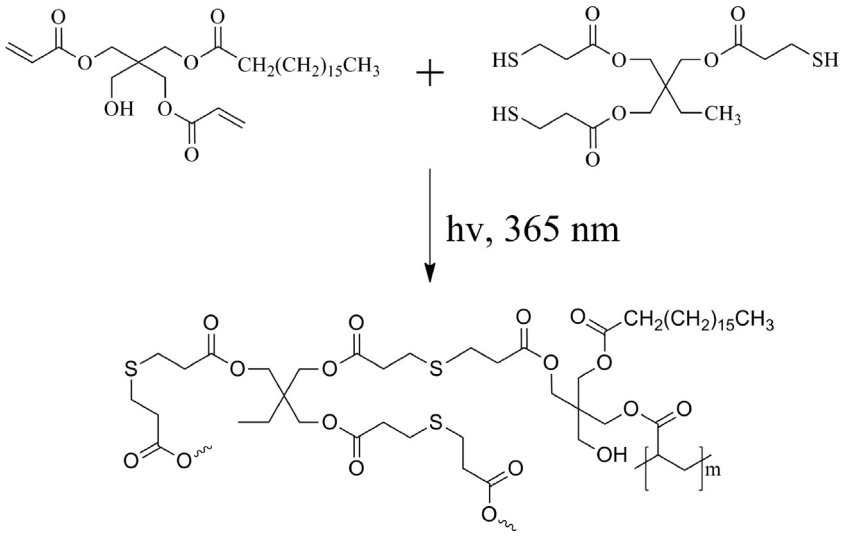

Fig. 1. The schematic preparation of poly(PEDAS-*co*-TPTM) monolith *via* thiol-acrylate polymerization.

PPMs are usually prepared by thermal- or photo-initiated radical polymerization of monovinyl and crosslinking divinyl monomers in the presence of porogenic solvents. A large number of monomers are available for preparation of polymeric monoliths with a variety of surface chemistries [23–26]. The most convenient and simple way to obtain the desired surface chemistry is the direct synthesis by using a single functional monomer and a crosslinker, such as divinylbenzene, ethylene dimethacrylate (EDMA), methylene bisacrylamide, poly(ethylene) diacrylate, bisphenol A dimetacrylate and bisphenol A ethoxylate diacrylate. The monomer of pentaerythritol diacrylate monostearate (PEDAS) (Fig. 1), having a C17-alkyl chain, two acrylate groups and one hydroxyl group, has been selected as the crosslinker to copolymerize with other monomers for preparation of anionic, cationic and neutral PPMs and widely applied in both CEC [27–31] and μLC [32,33]. However, they exhibited relatively low efficiency (46,000 plates/m at a linear flow rate of 0.85 mm/s) in μLC.

Photopolymerization of multifunctional thiols and enes is an efficient method for rapid preparation of films and plastics with unprecedented physical and mechanical properties because the polymerization occurs in air almost as rapidly as in an inert atmosphere, which is one of obstacles in traditional free radical polymerization [34,35]. Herein, a multi-thiol monomer, trimethylolpropane tris(3-mercaptopropionate) (TPTM) (Fig. 1), was selected, and thiol-based photopolymerization approach was first adopted to fabricate poly(PEDAS-*co*-TPTM) monoliths. Compared with the morphology of poly(PEDAS) monolith, those of poly(PEDAS-*co*-TPTM) monoliths were remarkably changed, leading to the improvement of both permeability and separation efficiency for small molecules in μLC.

2. Experimental

2.1. Reagents and materials

PEDAS, TPTM, methacryloxypropyl trimethoxysilane (γ-MAPS) (≥98%), 2,2-dimethoxy-2-phenylacetophenone (DMPA), bovine serum albumin (BSA), myoglobin (horse heart), ovalbumin, α-casein and polystyrene standards were purchased from Sigma (St Louis, MO, USA). Dithiothreitol (DTT) and iodoacetamide (IAA) were products of Sino-American Biotechnology Corporation (Beijing, China). Ethylene glycol, *n*-hexanol, ethanol, thiourea, benzene, toluene, ethylbenzene, propylbenzene, butylbenzene, phloroglucinol, catechol, phenol, *m*-cresol, 2,6-xylenol, caffeine,

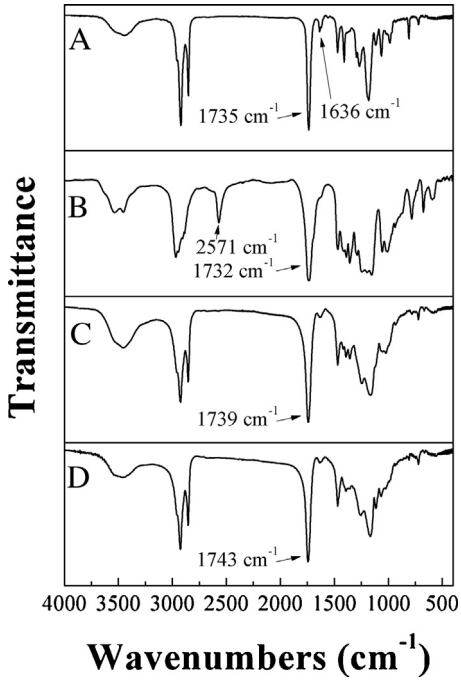

Fig. 2. FT-IR spectra of (A) PEDAS, (B) TPTM, (C) poly(PEDAS-*co*-TPTM) monolith and (D) poly(PEDAS) monolith.

1,4-phenylenediamine, benzidine, carbamazepine, *o*-nitroaniline and other standard analytes were of analytical grade, and obtained from Tianjin Kermel Chemical Plant (Tianjin, China). Methanol, acetonitrile (ACN) and tetrahydrofuran (THF) were HPLC-grade and acquired from Merck (Darmstadt, Germany). Deionized water was prepared with a Milli-Q system (Milli-pore, MA, USA). A UV-transparent fused-silica capillary with 75 μm i.d. and a polyimide coated fused-silica capillary with 50 μm i.d. were the products of Reafine Chromatography Ltd. (Hebei, China).

2.2. Instrumentation

The photopolymerization was performed in a UV-curing instrument (XL-1500A, λ = 365 nm, Spectronics Corporation, New York, USA). The microscopic image and energy-dispersive X-ray spectrum (EDX) of monolithic materials were obtained by scanning

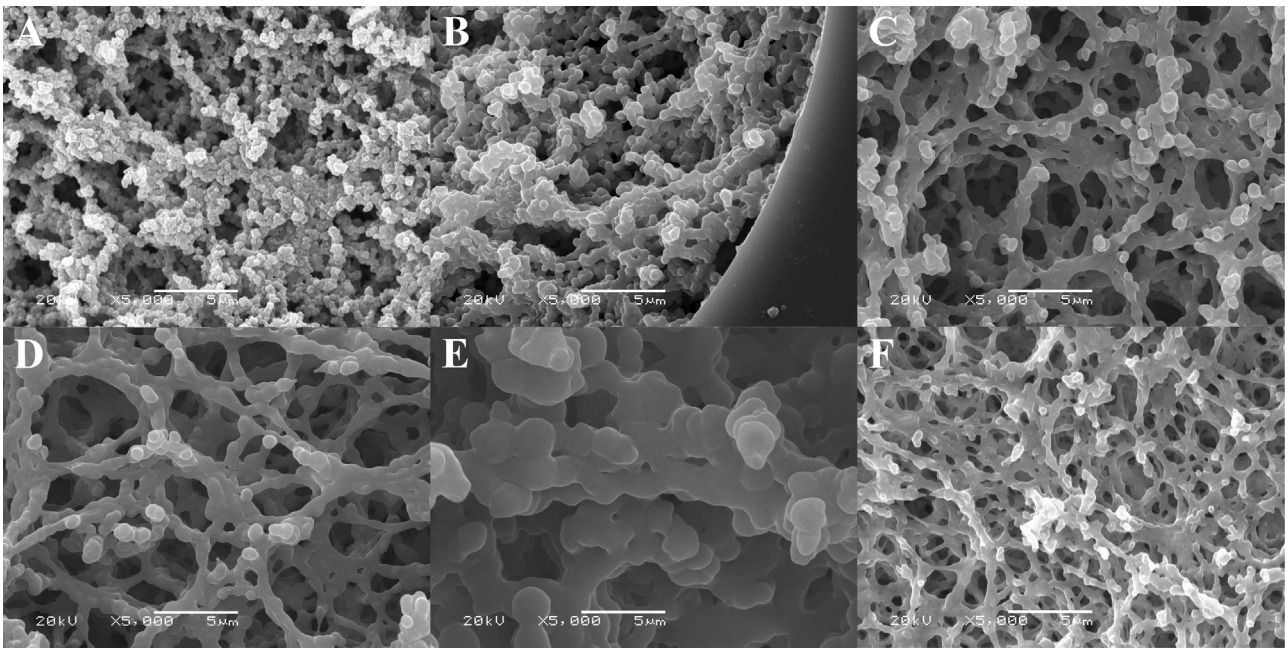

Fig. 3. SEM images of poly(PEDAS) and poly(PEDAS-*co*-TPTM) monoliths. (A) Column II, (B) column V, (C) column VII, (D) column VIII, (E) column IX and (F) column XI. Magnification: 5000×.

electron microscopy (SEM, JEOL JSM-5600, Tokyo, Japan). Fourier-transformed infrared spectroscopy (FT-IR) characterization was carried out on a Thermo Nicolet 380 spectrometer using KBr pellets (Nicolet, Wisconsin, USA). Thermogravimetry (TG) data were collected on a Setsys 16/18 (Setaram, Caluire, France).

The μLC experiments were performed on a LC system coupled with an Agilent 1100 micropump, a 7725i injector with a 20 μL sample loop and a K-2501 UV detector (Knauer, Berlin, Germany). A T-union connector was used as a splitter, with one end connected to the monolithic column and the other connected to a blank capillary (150 cm × 50 μm i.d.). The detection window was made by removing the polyimide coating of fused-silica capillary tubing. All chromatographic data were collected and analyzed using the software program HW-2000 from Qianpu Software (Shanghai, China).

Size-exclusion chromatography (SEC) on polymeric monoliths was carried out by using a LC10AT pump (Shimadzu, Kyoto, Japan), a 7725i injector and a K-2501 UV detector from Knauer (Berlin, Germany). All experiments were performed with THF as the mobile phase at the flow rate of 0.1 mL/min. Polystyrene standards with a molecular weight ranging from 800 to 900,000 Da were dissolved in THF. Benzene was adopted for the evaluation of the total porosity of the columns. The UV detection was set at 214 nm.

To inspect the permeability of the monoliths, pressure drop measurements were carried out on an Eksigent one dimensional Plus Nano-HPLC system (Eksigent, Dublin) at room temperature using ACN as the mobile phase. The permeability was calculated according to Darcy's Law by the following, $B_0 = F\eta L/(\pi r^2 \Delta P)$, where F (m^3/s) is the flow rate of the mobile phase, η is the viscosity of the mobile phase, L and r (m) are the effective length and inner radius of the column, ΔP (Pa) is the pressure drop of the column. The retention factor (k) was defined as $(t_r - t_0)/t_0$, where t_r and t_0 represent the retention times of the analytes and thiourea in this work, respectively.

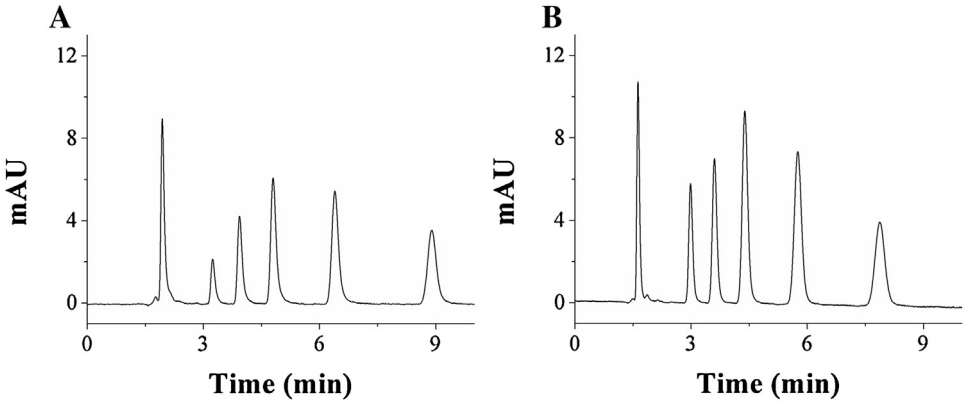

Fig. 4. Separation of alkylbenzenes in μLC on poly(PEDAS) (A) and poly(PEDAS-*co*-TPTM) (B) monoliths. The analytes are thiourea, benzene, toluene, ethylbenzene, propylbenzene and butylbenzene with different concentrations. The mobile phase was 60% (v/v) ACN/H_2O, and the flow rate was 175 μL/min (before split). The split ratio of column II and VII were 581 and 353, respectively. Column dimensions: column II, 17.5 cm × 75 μm i.d.; column VII, 25.8 cm × 75 μm i.d. On-column UV detection at 214 nm.

2.3. Preparation of monolithic columns and bulk monoliths via photo-initiated polymerization reaction

Before preparing monolithic columns, the inner wall of UV-transparent fused-silica capillary was pretreated and modified with γ-MAPS for anchoring monolith matrix. Briefly, the capillary was rinsed using 0.1 mol L^{-1} NaOH, water, 0.1 mol L^{-1} HCl and water for 2 h, successively. After being dried under nitrogen stream, the capillary was filled with γ-MAPS solution in methanol (50%, v/v), sealed with rubbers at both ends and submerged in water bath at 50 °C for 12 h. Finally, the capillary was rinsed with methanol to flush out the residual reagent and dried under nitrogen flow.

For preparation of poly(PEDAS) monoliths, the prepolymerization solution containing PEDAS (51.0 mg, 0.1 mmol), *n*-hexanol and ethylene glycol (as listed in Table 1) was mixed in a small transparent glass vial and sonicated for 15 min. Then 1.5 μL DMPA/*n*-hexanol (0.4 mol L^{-1}) solution was added. The obtained prepolymerization mixture was further sonicated for 2 min and introduced into the pretreated capillary with a certain length by a syringe. After sealing both ends with rubbers, the capillary was irradiated with UV light (λ = 365 nm, 120 mJ cm^{-2}) for 10 min. The resulting monolithic columns were then flushed with methanol to remove residuals.

For preparation of poly(PEDAS-*co*-TPTM) monoliths, the prepolymerization solution containing PEDAS (51.0 mg, 0.1 mmol), *n*-hexanol and ethylene glycol (as listed in Table 1) was mixed in a small transparent glass vial and sonicated for 15 min. Then an amount of TPTM (as listed in Table 1) and 1.5 μL DMPA/*n*-hexanol (0.4 mol L^{-1}) were also added. The resulting prepolymerization mixture was further sonicated for 2 min and introduced into the pretreated capillary with a certain length by a syringe. Poly(PEDAS-*co*-TPTM) monoliths were finally prepared as the above-mentioned procedures for preparation of poly(PEDAS) monoliths.

Bulk monoliths were polymerized by irradiation of the UV-transparent centrifuge tube (4 mL) with UV light (λ = 365 nm, 120 mJ cm^{-2}) for 10 min. To remove the residuals, the synthesized matrix was dipped into ethanol for 3 days, and repeated for 4 times. For the calculation of the polymer conversion, the obtained materials were dried under vacuum at 60 °C for 24 h. The polymer conversion of monolithic materials was determined according to the following equation: polymer conversion = weight material (dry)/weight precursors × 100%. For FT-IR characterization or TG analysis, the bulk monoliths were cut into small pieces and ground using mortar and pestle. Then the ground powders were dried in a vacuum at 60 °C for 24 h.

2.4. Tryptic digestion of four proteins and μLC-MS/MS Analysis

The tryptic digest procedure of four proteins (BSA, myoglobin, ovalbumin and α-casein) was according to that previously reported by us with minor modifications [36]. The 2 mg of four proteins (BSA, myoglobin, ovalbumin, α-casein) and 1 mL of denaturing buffer containing 8 mol/L urea and 0.1 mol/L ammonium bicarbonate were added into a 10 mL centrifuge tube. After the addition of 20 μL DTT (50 mmol L^{-1}), the mixture was incubated at 60 °C for 1 h. After that, 3.7 mg IAA was added, and the mixture was then incubated at room temperature in the dark for 40 min. Finally, the mixture was diluted 8-fold with 0.1 mol L^{-1} ammonium bicarbonate buffer (pH 8.2) and digested at 37 °C for 20 h with trypsin at the enzymeto-substrate ratio of 1:40 (w/w). After digestion, the pH value of the obtained tryptic digest solution was adjusted to 2.7 by 10% TFA aqueous solution. Followed by a solid-phase extraction (SPE) of the tryptic digest with a homemade C18 cartridge, the collected peptides elution was dried under vacuum and dissolved into a 0.1% formic acid aqueous solution (1 mL), and then stored in a −20 °C freezer before μLC-MS/MS analysis.

The tryptic digest was separated on a micro ultra-performance (μUPLC) system (Waters Corp., Milford, MA). Mobile phase A was water (0.1% formic acid), and mobile phase B was ACN (0.1% formic acid). An online C18 trap column (2 cm × 200 μm i.d., 5 μm C18 particulate, Waters Corp.) was used for sample injection. The tryptic digest of four proteins was automatically injected onto the trap column at a flow rate of 5 μL/min for 20 min with mobile phase A. After that, the trapped peptides were then separated at a flow rate of 100 μL/min on a polymeric monolith (column VII) or a packed column with an integrated emitter, which was prepared by directly tapering the tip from the outlet of the monolith (or the packed column) according to the previously reported approach [37]. The outlet of the monolith (or the packed column) was heated to adhere to a bare capillary by using a flame torch, and the tapered tip from the monolith (or the packed column) was prepared by drawing the bare capillary. Then an orifice diameter of 3–5 μm was cut, and the monolith (or the packed column) with an integrated emitter was ready for use.

3. Results and discussion

3.1. Preparation of poly(PEDAS)-based PPMs via photo-initiation mode

The poly(PEDAS)-based monolithic column has been prepared *via* free radical polymerization by several researchers [27–33]. In order to dissolve PEDAS, a binary porogenic system of *n*-hexanol/ethylene glycol was generally utilized for preparation of polymeric monoliths. In our case, poly(PEDAS) monoliths were initially prepared *via* photo-induced free radical polymerization using PEDAS as the sole monomer (as columns I–III, Table 1). It could be observed that the permeability of poly(PEDAS) monoliths slightly decreased from 1.17 to 0.64×10^{-14} m^2 when the content of *n*-hexanol increased from 155 to 165 μL, indicating that *n*-hexanol served as a microporogenic solvent, while ethylene glycol as a macroporogenic solvent. The permeability of poly(PEDAS) monolith was far lower than those of other common polymethacrylate [31], polystyrene [38] and polyacrylate [39] monoliths, which was not satisfied even if the preparation conditions were further optimized.

More recently, photoinitiated thiol-acrylate polymerization was exploited for preparation of hybrid monolithic columns, in which the acrylate not only homopolymerized, but also coupled with the thiol [36]. This offered a simple way to fabricate various PPMs. As a result, we had a try to add a few multi-thiol monomer (TPTM) into the prepolymerization solution of poly(PEDAS) monoliths. Compared with the permeabilities of poly(PEDAS) monoliths, those of the resulting poly(PEDAS-*co*-TPTM) monoliths were remarkably improved, and the results were given in Table 1. As for columns IV–VIII, they were fabricated with the same prepolymerization solution except that the amount of TPTM was different. It could be found that the permeabilities of poly(PEDAS-*co*-TPTM) monoliths dramatically increased from 1.41 to 3.67×10^{-14} m^2 when more and more TPTM was added into the prepolymerization solution. As for column IV, the amount of TPTM was 4 mg (thiol/vinyl, 0.15/1.0, mol/mol). As a result, most of PEDAS homopolymerized, and a little part of PEDAS would participate in copolymerization with TPTM [34,35]. With an increase of thiol monomer, more PEDAS would take part in the thiol-acrylate addition reaction. When the amount of TPTM was 20 mg (thiol/vinyl, 0.75/1.0, column VIII), it was possible that the formation of poly(PEDAS-*co*-TPTM) monolith was dominantly controlled by thiol-acrylate addition reaction mechanism, changing the pore structure and morphology of poly(PEDAS)-based monoliths, which was in favor of the enhancement of permeability. However, the permeability

Table 1
Composition of the polymerization mixtures for the preparation of PEDAS-based monolithic columns.

Column[a]	TPTM (mg)	*n*-Hexanol (μL)	Ethylene glycol (μL)	Permeability ($\times 10^{-14}$ m^2)
I	–	155	25	1.17
II	–	160	20	0.92
III	–	165	15	0.64
IV	4	160	20	1.41
V	8	160	20	1.68
VI	12	160	20	1.82
VII	16	160	20	2.25
VIII	20	160	20	3.67
IX	24	160	20	1.57
X	16	155	25	4.92
XI	16	165	15	0.73

[a] The 51 mg PEDAS and 1.5 μL DMPA/*n*-hexanol solution (0.4 mol L^{-1}) were added.

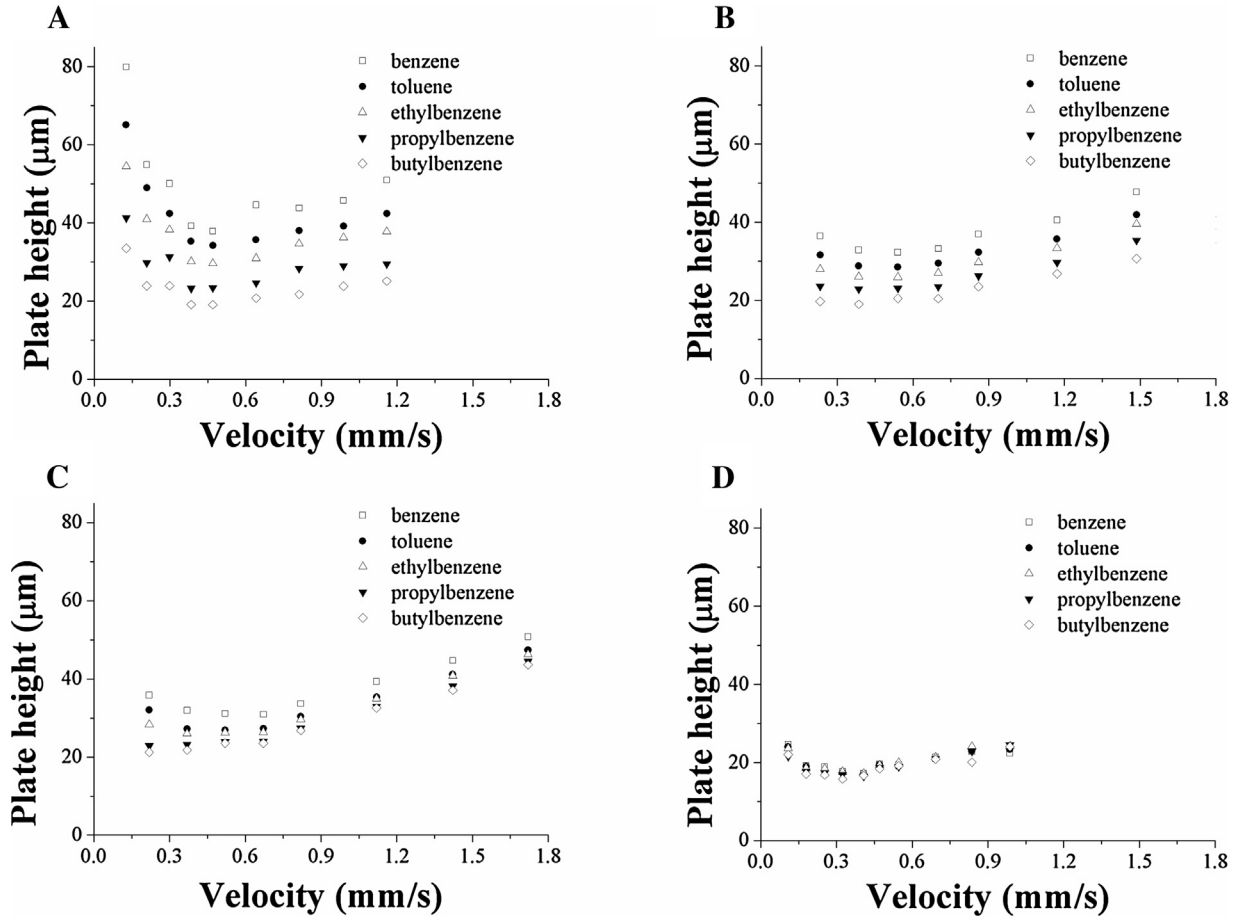

Fig. 5. The dependence of plate height of five alkylbenzenes on the linear velocity of mobile phase on (A) poly(PEDAS) and (B–D) poly(PEDAS-*co*-TPTM) monoliths. (A) column II, (B) column V, (C) column VII and (D) column XI. The mobile phase was 60% (v/v) ACN/H_2O. The flow rates, column II, from 15 to 175 μL/min (before split); columns V and XI, from 15 to 135 μL/min (before split); column VII, from 15 to 115 μL/min (before split). Column dimensions: column II, 17.5 cm × 75 μm i.d.; column V, 21.8 cm × 75 μm i.d.; column VII, 25.8 cm × 75 μm i.d.; column XI, 19.5 cm × 75 μm i.d. On-column UV detection at 214 nm.

of poly(PEDAS-*co*-TPTM) monolith decreased to 1.57×10^{-14} m^2 when the amount of TPTM was 24 mg (thiol/vinyl, 0.90/1.0, column IX). It was probably related to the remarkable increase of the total content of precursors (PEDAS and TPTM), which reached 33.0% (w/w).

The effect of the composition of porogenic system on the permeability of poly(PEDAS-*co*-TPTM) monoliths was also investigated. As for columns X, VII and XI, the permeability also decreased from 4.92 to 0.73×10^{-14} m^2 when the content of *n*-hexanol increased from 155 to 165 μL. Thus, it was also deduced that *n*-hexanol served as a microporogenic solvent, while ethylene glycol as a macroporogenic solvent. In a word, the permeability of poly(PEDAS-*co*-TPTM) monoliths could be enhanced by adding a few TPTM when compared with those of poly(PEDAS) monoliths, which were prepared with the same porogenic system (columns II and IV–IX). In addition, the polymer conversions of poly(PEDAS) (column II) and poly(PEDAS-*co*-TPTM) monoliths (column VII) were measured, and reached 94.6% and 93.2%, respectively, indicating that two kinds of monoliths might be efficiently crosslinked by either homopolymerization of PEDAS or thiol-acrylate polymerization of PEDAS and TPTM.

The repeatabilities of both poly(PEDAS) (column II) and poly(PEDAS-*co*-TPTM) (column VII) monoliths were evaluated through the RSD for retention factor (*k*) of benzene as a model

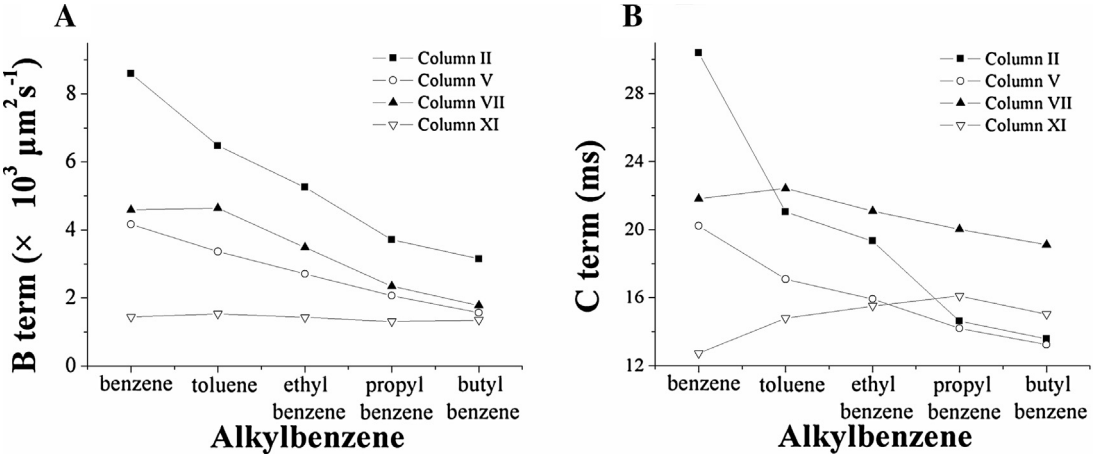

Fig. 6. The relationships of (A) B- and (B) C-terms obtained from the van Deemter curves on four monoliths with alkylbenzenes.

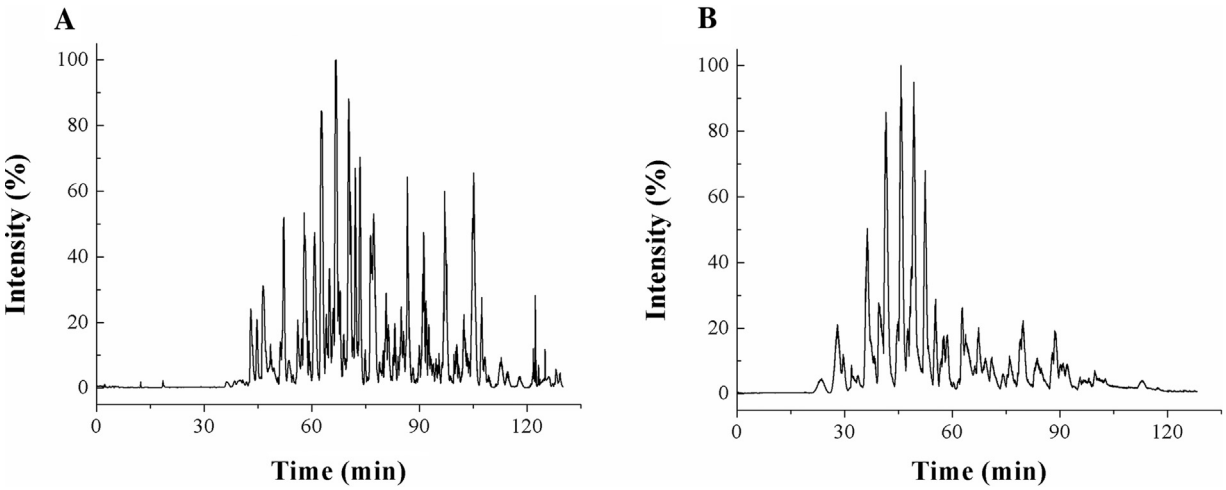

Fig. 7. Chromatograms of tryptic digest of four proteins (BSA, myoglobin, ovalbumin, and α-casein) on packed column and poly(PEDAS-*co*-TPTM) monolith in μLC-MS/MS analysis. Experimental conditions: (A) C18 packed column, (B) column VII. Column dimension, C18 packed column, 20 cm × 75 μm i.d.; column VII, 42 cm × 75 μm i.d. Mobile phase A, 0.1% formic acid in water, mobile phase B, 0.1% formic acid in ACN; the gradient was 0–5% ACN in 2 min, 5–35% ACN in 104 min, 35–80% ACN in 2 min, retained 80% ACN for 10 min; flow rate, 100 μL/min. Protein sequence coverage: (A) BSA (73%), myoglobin (57%), ovalbumin (34%), α-casein (31%); (B) BSA (62%), myoglobin (57%), ovalbumin (51%), α-casein (33%).

analyte (thiourea as the viod time marker) in μLC. The run-to-run repeatabilities were 0.8% ($n = 4$) and 0.6% ($n = 5$), respectively. Besides, the batch-to-batch repeatability was also investigated, which gave RSD values of 1.8% ($n = 3$) and 2.1% ($n = 3$), respectively, indicating satisfactory repeatability for preparation of two polymeric monoliths.

3.2. Characterization of PPMs

Fig. 2 shows the FT-IR spectra of PEDAS, TPTM, poly(PEDAS-*co*-TPTM) and poly(PEDAS) monoliths. The peaks at 1735 and 1636 cm^{-1} (Fig. 2A) indicated the existence of α,β-unsaturated carbonyl in PEDAS, while the peak at 2571 cm^{-1} (Fig. 2B) was assigned to thiol groups in TPTM. In the spectrum of poly(PEDAS-*co*-TPTM) monolith (Fig. 2C), the peak signal at 1735 cm^{-1} was changed to 1739 cm^{-1}, and the intensity of the peak at 1636 cm^{-1} was remarkably decreased. Additionally, the distinct thiol signal in TPTM (2571 cm^{-1} in Fig. 2B) disappeared in Fig. 2C. These results indicated that thiol-acrylate polymerization of PEDAS and TPTM was carried out in the formation of poly(PEDAS-*co*-TPTM) monolith. Meanwhile, as shown in Fig. 2D, the shift of the carbonyl signal from 1735 to 1743 cm^{-1} and the decrease of the peak intensity at 1636 cm^{-1} suggested the traditional free radical polymerization of acrylate groups in PEDAS was successfully performed during the synthesis of poly(PEDAS) monolith, in which α,β-unsaturated carbonyl was transformed to saturated carbonyl.

Thermal stability of poly(PEDAS) and poly(PEDAS-*co*-TPTM) monoliths is illustrated by TGA curves (Fig. S1), which were measured at a heating rate of 10 K/min from 308 to 1073 K under flowing argon. The results exhibited that both poly(PEDAS) and poly(PEDAS-*co*-TPTM) monoliths lost weight from 593 to 763 K, exhibiting similar thermal stability of two monoliths. Fig. S2 shows a good linear relationship of back pressure against flow rate even at the high pressure of 35 MPa, implying that both two organic monoliths possessed relatively good mechanical stability. Fig. S3 shows the energy-dispersive X-ray spectrums (EDX) of poly(PEDAS) and poly(PEDAS-*co*-TPTM) monoliths. The peaks of elemental carbon and oxygen appeared in the EDX of poly(PEDAS) monolith (Fig. S3A). Apart from these two elements, the peak of elemental sulfur also appeared in the EDX of poly(PEDAS-*co*-TPTM) monolith (Fig. S3B), indicating the incorporation of thiol-containing crosslinker. Particularly, due to the shrinkage of both dried poly(PEDAS) and poly(PEDAS-*co*-TPTM) monoliths (Fig. S4), it is not suitable for the mercury intrusion porosimetry (MIP) and nitrogen adsorption/desorption measurements on these two monoliths.

The hydrodynamic diameters of benzene and the largest polystyrene standard (Mr = 900,000) used in this study are calculated to be 0.32 and 78.0 nm according to the equation [40]: $R = 0.0246Mr^{0.588}$, where the hydrodynamic diameter, R, is in nanometer. In SEC measurement, benzene can penetrate into all pores larger than 0.32 nm and the polystyrene standard with Mr = 900,000 (V_0) is expected to be excluded from pores smaller than 78.0 nm. Usually, the retention volume of benzene is considered as the total pore volume. The total porosity, $\varepsilon_T = V_M/V_C$, is calculated from the elution volumes of benzene, V_M, and the geometrical volumes of the empty columns, V_C. In addition, the external porosity, $\varepsilon_0 = V_0/V_C$, is determined from the elution volume of the polystyrene standard with Mr = 900,000 (V_0). As shown in Fig. S5, ε_T and ε_0 of poly(PEDAS) monolith (column II) were calculated to 89.9% and 58.3%, respectively. However, the swelling of poly(PEDAS-*co*-TPTM) monoliths in THF was observed, and THF as the mobile phase could not flow through them. As a result, SEC on poly(PEDAS-*co*-TPTM) monoliths could not be carried out. The remarkable compression of poly(PEDAS-*co*-TPTM) monoliths could be also observed from the photos of bulk poly(PEDAS-*co*-TPTM) monolith, which changed from white (Fig. S4C) to semitransparent (Fig. S4D) after drying treatment.

The morphologies of poly(PEDAS) and poly(PEDAS-*co*-TPTM) monoliths are characterized by SEM (Fig. 3 and S6). Fig. 3A shows the cauliflower-like globular structure of poly(PEDAS) monolith (column II), which is intricated by typically micrometer-sized pores. When a small amount of TPTM (8 mg) was added into the prepolymerized solution, poly(PEDAS-*co*-TPTM) monolith (column V) exhibited a similar morphology (Fig. 3B) with poly(PEDAS) monolith (column II). It could be deduced that the homopolymerization of acrylates is the main reaction during the synthesis of this poly(PEDAS-*co*-TPTM) monolith. As the amount of TPTM further increased to 16, 20 and 24 mg, the morphologies of poly(PEDAS-*co*-TPTM) monoliths seemed rather different from those of poly(PEDAS) monoliths. As shown in Fig. 3C–E, the reticulated bicontinuous structure could be used to depict the morphologies of these poly(PEDAS-*co*-TPTM) monoliths (columns VII–IX). Such bicontinuous structure of poly(PEDAS-*co*-TPTM) monoliths was very similar with the morphologies of those hybrid monoliths synthesized *via* epoxy-amine ring-opening polymerization [41]. The difference between the morphologies of poly(PEDAS) and poly(PEDAS-*co*-TPTM) monoliths is possibly attributed to the transition from free radical chain-growth to step-growth polymerization of thiol-acrylate additional reaction, resulting in different phase separation process. Two poly(PEDAS-*co*-TPTM) monoliths (column VII and XI) were fabricated with the same amount of monomer but different composition of porogenic solvents. It could be observed from Fig. 3C and F that the column XI possessed thinner skeleton and smaller through-pore. The higher content of microporogenic solvent (*n*-hexanol) in polymerization solution might delay the phase separation, affecting the domain size of poly(PEDAS-*co*-TPTM) monolith.

3.3. Chromatographic performance

The chromatographic properties of poly(PEDAS) and poly(PEDAS-*co*-TPTM) monoliths were evaluated by μLC separation of alkylbenzenes as probes. As shown in Fig. 4A and B, alkylbenzenes were baseline-separated on both poly(PEDAS) (column II) and poly(PEDAS-*co*-TPTM) monoliths (column VII) with the mobile phase of ACN/water (60/40, v/v) at the flow rate of 175 μL/min (before split) and eluted in the order of their hydrophobicities. The split ratio of columns II and VII were 581 and 353, respectively. Furthermore, a decrease in retention was evidenced as the ACN content increased from 50% to 80% (Fig. S7A and B), also demonstrating the reversed-phase retention mechanism of alkylbenzenes on two monoliths. The C17-alkyl chain of PEDAS could contribute to the hydrophobic property of them.

The efficiency evaluation for poly(PEDAS) and poly(PEDAS-*co*-TPTM) monoliths was performed by plotting the plate height of five alkylbenzenes *versus* the linear velocity of mobile phase in μLC. As depicted in Fig. 5A, the minimum plate heights for alkylbenzenes on poly(PEDAS) monolith (column II) were ranged in 19.1–37.9 μm at the velocity of 0.47 mm/s. When a small amount of TPTM (8 mg) was added, minimum plate heights for alkylbenzenes on poly(PEDAS-*co*-TPTM) monolith (column V, Fig. 5B) were in the range of 19.0–33.2 μm at the velocity of 0.39 mm/s. As the TPTM was further added (16 mg), minimum plate heights for alkylbenzenes on poly(PEDAS-*co*-TPTM) monolith (column VII, Fig. 5C) were between 21.2–35.8 μm (at 0.22 mm/s). It could be concluded that the optimum velocity of the monoliths decreased accordingly with an increase of TPTM. In addition, when the composition of porogenic solvents was adjusted, the resulting poly(PEDAS-*co*-TPTM) monolith (column XI) exhibited much lower plate heights (15.7–17.7 μm, at 0.32 mm/s). Furthermore, it could be observed that the plate heights for weak-retained compounds (such as benzene) were higher than those of strong-retained compounds (such as butylbenzene). These results demonstrated a retention-independent efficient performance for small molecule separation on poly(PEDAS) and poly(PEDAS-*co*-TPTM) monoliths. On one hand, an unexpected effect of extra-column volumes might impair more column efficiencies of weak-retained compounds than strong-retained compounds [42]. On the other hand, the hyper-crosslinking degree of poly(PEDAS) monolith might impede the generation of gel porosity probed by small molecules, reducing the mass transfer resistance [38]. Also, the bicontinuous structure of poly(PEDAS-*co*-TPTM) monoliths would provide a shorter diffusion distance and greatly accelerate the mass transfer, leading to a lower C-term [43–46].

The values of A-, B- and C-terms in the van Deemter equation, which represent eddy dispersion, longitudinal diffusion, and mass transfer resistance, respectively, were obtained by nonlinearly fitting the plate height curves of poly(PEDAS) and poly(PEDAS-*co*-TPTM) monoliths. The A-terms of these monoliths are not discussed here due to their unregularity. The relationships of B- and C-terms on four monoliths with hydrophobicity of alkylbenzenes are shown in Fig. 6. It could be found that B-terms of poly(PEDAS) monolith (column II) decreased from 8.60 to 3.15×10^3 μm^2 s^{-1} with an increase of hydrophobicity of alkylbenzenes, while B-terms of poly(PEDAS-*co*-TPTM) monoliths (columns V, VII and XI) decreased more gently. Especially, B-terms of alkylbenzenes for column XI were almost kept as a constant, which slightly varied from 1.53 (benzene) to 1.31×10^3 μm^2 s^{-1} (butylbenzene). In addition, B-terms of poly(PEDAS) monolith (column II) were higher than those of poly(PEDAS-*co*-TPTM) monoliths (columns V, VII and XI). Similarly, C-terms of poly(PEDAS) monolith (column II) also decreased more dramatically (from 30.4 to 13.6 ms) than those of poly(PEDAS-*co*-TPTM) monoliths (columns V, VII and XI). However, C-terms of benzene and butylbenzene were 12.7 and 15.0 ms for column XI, respectively. Both B- and C-terms for poly(PEDAS) and poly(PEDAS-*co*-TPTM) monoliths might be closely related with their morphologies and pore structures. The bicontinuous structure of poly(PEDAS-*co*-TPTM) monoliths and the cauliflower-like globular structure of poly(PEDAS) monoliths played vital influences on the communication of the small molecules and the stationary phase, leading to differential B- and C-terms.

3.4. Application of PPMs

Fig. S8 presents the separations of phenols and basic compounds on poly(PEDAS-*co*-TPTM) monoliths by μLC, which were baseline

separated. Besides the separations of these small molecules, the separation of complex sample, a tryptic digest of four proteins (BSA, myoglobin, ovalbumin and α-casein), was also performed on poly(PEDAS-*co*-TPTM) monolith by μLC-MS/MS. As a comparison, a packed column was also investigated in the separation of the tryptic digest of these four proteins. The chromatograms are illustrated in Fig. 7. Based on the database search of the chromatogram, 82 unique peptides were positively identified with protein sequence coverages (BSA 73%, myoglobin 57%, ovalbumin 34% and α-casein 31%) on packed column (Fig. 7A), while 66 unique peptides were positively identified with protein sequence coverages (BSA 62%, myoglobin 57%, ovalbumin 51% and α-casein 33%) on poly(PEDAS-*co*-TPTM) monolith (Fig. 7B). Although the separation performance on poly(PEDAS-*co*-TPTM) monolith is not as good as that on packed column, the good permeability and low back pressure of poly(PEDAS-*co*-TPTM) monolith could enable the use of longer columns, thereby achieving higher column efficiency and separation performance. All these results demonstrated the potential of poly(PEDAS-*co*-TPTM) monoliths in the analysis of complex biosamples.

4. Conclusion

A novel approach of photo-initiated thiol-acrylate polymerization was employed for preparation of polymeric monoliths. The results indicated rapid reaction and high conversion of the corresponding monomers in thiol-acrylate polymerization. The obtained poly(PEDAS-*co*-TPTM) monolith exhibited homogeneous bicontinuous structure, which was distinct from cauliflower-like globular structure of poly(PEDAS) monolith prepared *via* traditional free radical polymerization. Compared with poly(PEDAS) monolith, poly(PEDAS-*co*-TPTM) monolith possessed better permeability when they were synthesized under the same preparation conditions. Besides, by adjusting the composition of porogenic solvents, poly(PEDAS-*co*-TPTM) monolith could exhibit lower plate heights for alkylbenzenes than poly(PEDAS) monolith. In a word, thiol-acrylate polymerization is a feasible and useful approach for preparation of polymeric monoliths with high efficiency. It is anticipated that various commercially available acrylate monomers would be introduced to the fabrication of several polymeric monoliths by thiol-acrylate polymerization.

Acknowledgements

Financial support is gratefully acknowledged from the China State Key BasicResearch Program Grant (2013CB-911203, 2012CB910601), the National Natural Sciences Foundation of China (21235006), the Creative Research Group Project of NSFC (21321064), and the Knowledge Innovation program of DICP to H. Zou as well as the National Natural Sciences Foundation of China (No. 21175133 and 21575141) to J. Ou.

Appendix A. Supplementary data

Supplementary data associated with this article can be found, in the online version, at http://dx.doi.org/10.1016/j.chroma.2016.01.063.

References

[1] F. Svec, Y. Lv, Advances and recent trends in the field of monolithic columns for chromatography, Anal. Chem. 87 (2015) 250–273.
[2] G. Guiochon, Monolithic columns in high-performance liquid chromatography, J. Chromatogr. A 1168 (2007) 101–168.
[3] H.F. Zou, X.D. Huang, M.L. Ye, Q.Z. Luo, Monolithic stationary phases for liquid chromatography and capillary electrochromatography, J. Chromatogr. A 954 (2002) 5–32.
[4] F. Svec, Organic polymer monoliths as stationary phases for capillary HPLC, J. Sep. Sci. 27 (2004) 1419–1430.
[5] M.R. Buchmeiser, Polymeric monolithic materials: syntheses, properties, functionalization and applications, Polymer 48 (2007) 2187–2198.
[6] F. Svec, Recent developments in the field of monolithic stationary phases for capillary electrochromatography, J. Sep. Sci. 28 (2005) 729–745.
[7] F. Svec, Stellan Hjerten's contribution to the development of monolithic stationary phases, Electrophoresis 29 (2008) 1593–1603.
[8] H. Aoki, N. Tanaka, T. Kub, K. Hosoya, Polymer-based monolithic columns in capillary format tailored by using controlled in situ polymerization, J. Sep. Sci. 32 (2009) 341–358.
[9] R.D. Arrua, M. Talebi, T.J. Causon, E.F. Hilder, Review of recent advances in the preparation of organic polymer monoliths for liquid chromatography of large molecules, Anal. Chim. Acta 738 (2012) 1–12.
[10] J. Hernandez Borges, Z. Aturki, A. Rocco, S. Fanali, Recent applications in nanoliquid chromatography, J. Sep Sci. 30 (2007) 1589––1610.
[11] P. Jandera, Advances in the development of organic polymer monolithic columns and their applications in food analysis-A review, J. Chromatogr. A 1313 (2013) 37–53.
[12] J. Krenkova, F. Svec, Less common applications of monoliths: IV. Recent developments in immobilized enzyme reactors for proteomics and biotechnology, J. Sep. Sci. 32 (2009) 706–718.
[13] M. Rigobello Masini, J.C.P. Penteado, J.C. Masini, Monolithic columns in plant proteomics and metabolomics, Anal. Bioanal. Chem. 405 (2013) 2107–2122.
[14] E.G. Vlakh, T.B. Tennikova, Applications of polymethacrylate-based monoliths in high-performance liquid chromatography, J. Chromatogr. A 1216 (2009) 2637–2650.
[15] R. Wu, L.G. Hu, F.J. Wang, M.L. Ye, H. Zou, Recent development of monolithic stationary phases with emphasis on microscale chromatographic separation, J. Chromatogr. A 1184 (2008) 369–392.
[16] K. Liu, P. Aggarwal, J.S. Lawson, H.D. Tolley, M.L. Lee, Organic monoliths for high-performance reversed-phase liquid chromatography, J. Sep. Sci. 36 (2013) 2767–2781.
[17] F. Svec, Quest for organic polymer-based monolithic columns affording enhanced efficiency in high performance liquid chromatography separations of small molecules in isocratic mode, J. Chromatogr. A 1228 (2012) 250–262.
[18] S. Eeltink, F. Svec, Recent advances in the control of morphology and surface chemistry of porous polymer-based monolithic stationary phases and their application in CEC, Electrophoresis 28 (2007) 137–147.
[19] Y.Q. Lv, F.M. Alejandro, J.M.J. Frechet, F. Svec, Preparation of porous polymer monoliths featuring enhanced surface coverage with gold nanoparticles, J. Chromatogr. A 1261 (2012) 121–128.
[20] J. Urban, P. Jandera, Recent advances in the design of organic polymer monoliths for reversed-phase and hydrophilic interaction chromatography separations of small molecules, Anal. Bioanal. Chem. 405 (2013) 2123–2131.
[21] J. Urban, F. Svec, J.M.J. Frechet, Hypercrosslinking New approach to porous polymer monolithic capillary columns with large surface area for the highly efficient separation of small molecules, J. Chromatogr. A 1217 (2010) 8212–8221.
[22] Y.Q. Lv, Z.X. Lin, F. Svec, Hypercrosslinked large surface area porous polymer monoliths for hydrophilic interaction liquid chromatography of small molecules featuring zwitterionic functionalities attached to gold nanoparticles held in layered structure, Anal. Chem. 84 (2012) 8457–8460.
[23] E.G. Vlakh, T.B. Tennikova, Preparation of methacrylate monoliths, J. Sep. Sci. 30 (2007) 2801–2813.
[24] J. Urban, P. Jandera, Polymethacrylate monolithic columns for capillary liquid chromatography, J. Sep. Sci. 31 (2008) 2521–2540.
[25] Z.D. Xu, L.M. Yang, Q.Q. Wang, Different alkyl dimethacrylate mediated stearyl methacrylate monoliths for improving separation efficiency of typical alkylbenzenes and proteins, J. Chromatogr. A 1216 (2009) 3098–3106.
[26] Y. Li, H.D. Tolley, M.L. Lee, Polyhydroxyethyl acrylate-co-poly(ethylene glycol) diacrylate monolithic column for efficient hydrophobic interaction chromatography of proteins, Anal. Chem. 81 (2009) 9416–9424.
[27] M. Bedair, Z. El Rassi, Capillary electrochromatography with monolithic stationary phases- II. Preparation of cationic stearyl-acrylate monoliths and their electrochromatographic characterization, J. Chromatogr. A 1013 (2003) 35–45.
[28] M. Bedair, Z. El Rassi, Capillary electrochromatography with monolithic stationary phases- III. Evaluation of the electrochromatographic retention of neutral and charged solutes on cationic stearyl-acrylate monoliths and the separation of water-soluble proteins and membrane proteins, J. Chromatogr. A 1013 (2003) 47–56.
[29] F.M. Okanda, M. El Rassi, Capillary electrochromatography with monolithic stationary phases. 4. Preparation of neutral stearyl-acrylate monoliths and their evaluation in capillary electrochromatography of neutral and charged small species as well as peptides and proteins, Electrophoresis 26 (2005) 1988–1995.
[30] M. Bedair, Z. El Rassi, Capillary electrochromatography with monolithic stationary phases: 1. Preparation of sulfonated stearyl acrylate monoliths and their electrochromatographic characterization with neutral and charged solutes, Electrophoresis 23 (2002) 2938–2948.
[31] P. Chaisuwan, D. Nacapricha, P. Wilairat, Z. Jiang, N.W. Smith, Separation of alpha- beta-, gamma-, delta-tocopherols and alpha-tocopherol acetate on a pentaerythritol diacrylate monostearate-ethylene dimethacrylate monolith by capillary electrochromatography, Electrophoresis 29 (2008) 2301–2309.

[32] Z.J. Jiang, N.W. Smith, P.D. Ferguson, M.R. Taylor, Mixed-mode reversed-phase and ion-exchange monolithic columns for micro-HPLC, J. Sep. Sci. 31 (2008) 2774–2783.
[33] Y. Li, H.D. Tolley, M.L. Lee, Preparation of monoliths from single crosslinking monomers for reversed-phase capillary chromatography of small molecules, J. Chromatogr. A 1218 (2011) 1399–1408.
[34] C.E. Hoyle, C.N. Bowman, Thiol-ene click chemistry, Angew. Chem. Int. Ed. 49 (2010) 1540–1573.
[35] C.E. Hoyle, T.Y. Lee, T. Roper, Thiol-enes: chemistry of the past with promise for the future, J. Polym. Sci. Part A: Polym. Chem. 42 (2004) 5301–5338.
[36] H.Y. Zhang, J.J. Ou, Z.S. Liu, H.W. Wang, Y.M. Wei, H.F. Zou, Preparation of hybrid monolithic columns via one-pot photoinitiated thiol-acrylate polymerization for retention-independent performance in capillary liquid chromatography, Anal. Chem. 87 (2015) 8789–8797.
[37] C. Xie, M. Ye, X. Jiang, W. Jin, H. Zou, Octadecylated silica monolith capillary column with integrated nanoelectrospray ionization emitter for highly efficient proteome analysis, Mol. Cell. Proteomics 5 (2006) 454–461.
[38] I. Nischang, I. Teasdale, O. Bruggemann, Towards porous polymer monoliths for the efficient, retention-independent performance in the isocratic separation of small molecules by means of nano-liquid chromatography, J. Chromatogr. A 1217 (2010) 7514–7522.
[39] A. Escrig Domenech, I. Ten Domenech, E.F. Simo Alfonso, J.M. Herrero Martinez, Preparation and characterization of octadecyl acrylate monoliths for capillary electrochromatography by photochemical thermal, and chemical initiation, J. Sep. Sci. 36 (2013) 2283–2290.
[40] J. Urban, S. Eeltink, P. Jandera, P.J. Schoenmakers, Characterization of polymer-based monolithic capillary columns by inverse size-exclusion chromatography and mercury-intrusion porosimetry, J. Chromatogr. A 1182 (2008) 161–168.
[41] H. Wang, J. Ou, H. Lin, Z. Liu, G. Huang, J. Dong, H. Zou, Chromatographic assessment of two hybrid monoliths prepared via epoxy-amine ring-opening polymerization and methacrylate-based free radical polymerization using methacrylate epoxy cyclosiloxane as functional monomer, J. Chromatogr. A 1367 (2014) 131–140.
[42] I. Nischang, On the chromatographic efficiency of analytical scale column format porous polymer monoliths: interplay of morphology and nanoscale gel porosity, J. Chromatogr. A 1236 (2012) 152–163.
[43] I. Nischang, Porous polymer monoliths: morphology, porous properties, polymer nanoscale gel structure and their impact on chromatographic performance, J. Chromatogr. A 1287 (2013) 39–58.
[44] F. Gritti, G. Guiochon, Mass transport of small retained molecules in polymer-based monolithic columns, J. Chromatogr. A 1362 (2014) 49–61.
[45] F. Gritti, G. Guiochon, Mass transfer kinetics, band broadening and column efficiency, J. Chromatogr. A 1221 (2012) 2–40.
[46] H. Lin, J. Ou, Z. Liu, H. Wang, J. Dong, H. Zou, Facile construction of macroporous hybrid monoliths via thiol-methacrylate Michael addition click reaction for capillary liquid chromatography, J. Chromatogr. A 1379 (2015) 34–42.